RSC Advances

PAPER

View Article Online
View Journal | View Issue

Cite this: *RSC Adv.*, 2023, **13**, 3438

Structure-based approach: molecular insight of pyranocumarins against α-glucosidase through computational studies†

Muhammad Ikhlas Abdjan,[ab] Nanik Siti Aminah, *[bc] Alfinda Novi Kristanti, [bc] Imam Siswanto,[ad] Baso Ilham,[b] Andika Pramudya Wardana[ab] and Yoshiaki Takaya[e]

α-glucosidase is an enzyme that catalyzes the release of α-glucose molecules through hydrolysis reactions. Regulation of this enzyme can increase sugar levels in type-2 diabetes mellitus (DM) patients. Pyranocoumarin derivatives have been identified as α-glucosidase inhibitors. Through an *in silico* approach, this work studied the inhibition of three pyranocoumarin compounds against the α-glucosidase at the molecular level. Molecular docking and molecular dynamics simulation were performed to understand the dynamics behavior of pyranocoumarin derivatives against α-glucosidase. The prediction of free binding energy (ΔG_{bind}) using the Quantum Mechanics/Molecular Mechanics-Generalized Born (QM/MM-GBSA) approach for each system had the following results, PC1-α-Glu: −13.97 kcal mol^{-1}, PC2-α-Glu: −3.69 kcal mol^{-1}, and PC3-α-Glu: −13.68 kcal mol^{-1}. The interaction energy of each system shows that the grid score, ΔG_{bind}, and ΔG_{exp} values had a similar correlation, that was PC1-α-Glu > PC3-α-Glu > PC2-α-Glu. Additionally, the decomposition energy analysis ($\Delta G_{bind}^{residue}$) was carried out to find out the contribution of the key binding residue. The results showed that there were 15 key binding residues responsible for stabilizing pyranocumarin binding with criteria of $\Delta G_{bind}^{residue}$ < −1.00 kcal mol^{-1}. The evaluation presented in this work could provide information on the molecular level about the inhibitory efficiency of pyranocoumarin derivatives against a-glucosidase enzyme based on computational studies.

Received 27th November 2022
Accepted 16th January 2023

DOI: 10.1039/d2ra07537g

rsc.li/rsc-advances

Introduction

α-Glucosidase is a carbohydrase enzyme that catalyzes the release of α-glucose molecules.[1] In general, several types of glucosidase are found in the small intestine, namely maltase-glucoamylase and sucrose-isomaltase, which play a role in the release of glucose monomers.[2] The glucosidase enzyme is located in the small intestine area, specifically in epithelial cells. Excessive activity of this enzyme causes the release of glucose which is absorbed by the small intestine lumen and enters through blood circulation. The glucose release causes blood sugar levels and uncontrolled hyperglycemia to increase in type-2 diabetes mellitus (DM) patients.[3] α-Glucosidase is one of the glucosidase enzymes, which is responsible for the mechanism of DM. α-glucosidase catalyzes the hydrolysis reaction in breaking the α -(1,4)-glycosidic linkage of carbohydrates to become a free monosaccharide (α-D-glucose) before it penetrates the bloodstream.[4] It has been reported that several inhibitors from small compounds can bind to the active site of a-glycosidase and delay the absorption of carbohydrates by the small intestine. It makes the α-glucosidase become an essential target in reducing blood sugar levels.[5–7] Inhibition of this enzyme is expected to reduce the process of releasing glucose from the breakdown of oligosaccharides and disaccharides into their monomers. Therefore, drug candidates are needed that can interfere with and inhibit the activity of this enzyme. The inhibitory mechanism can be studied through molecular studies on the α-glucosidase active site as a targeted protein.[4] Several previous studies stated that inhibition of the α-glucosidase was a promising main target in treating type-2 DM patients.[5–7]

Inhibition of the α-glucosidase is expected to stop its activity in breaking down carbohydrates into glucose molecules. It should be noted that α-glucosidase inhibitors are small molecules that act as competitive inhibitors.[8] The investigation for

[a]*Ph.D. Student of Mathematics and Natural Sciences, Faculty of Science and Technology, Universitas Airlangga, Komplek Kampus C UNAIR, Jl. Mulyorejo, 60115, Surabaya, Indonesia*

[b]*Department of Chemistry, Faculty of Science and Technology, Universitas Airlangga, Surabaya 60115, Indonesia. E-mail: nanik-s-a@fst.unair.ac.id*

[c]*Biotechnology of Tropical Medicinal Plants Research Group, Universitas Airlangga, Surabaya 60115, Indonesia*

[d]*Bioinformatic Laboratory, UCoE Research Center for Bio-Molecule Engineering Universitas Airlangga, Surabaya, Indonesia*

[e]*Faculty of Pharmacy, Meijo University, 150 Yagotoyama, Tempaku, Nagoya, 468-8503, Japan*

† Electronic supplementary information (ESI) available. See DOI: https://doi.org/10.1039/d2ra07537g

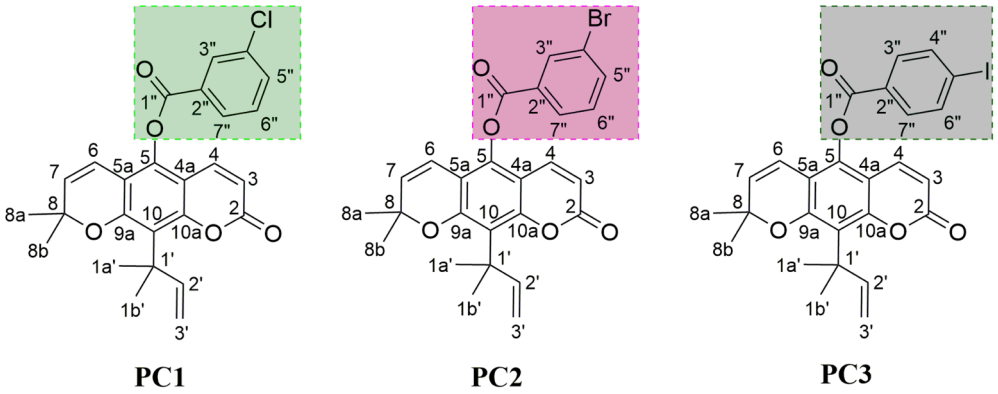

Fig. 1 The chemical structure of pyranocoumarin derivatives: 2,2-dimethyl-10-(2-methylbut-3-en-2-yl)-8-oxo-2*H*,8*H*-pyrano[3,2-g]chromen-5-yl 3-chlorobenzoate (PC1), 2,2-dimethyl-10-(2-methylbut-3-en-2-yl)-8-oxo-2*H*,8*H*-pyrano[3,2-g]chromen-5-yl 3-bromobenzoate (PC2), and 2,2-dimethyl-10-(2-methylbut-3-en-2-yl)-8-oxo-2*H*,8*H*-pyrano[3,2-g]chromen-5-yl 4-iodobenzoate (PC3).

candidate inhibitors that can bind to the active site is a promising opportunity to control the release of α-D-glucose molecules into epithelial cells.[9] Inhibition of α-glucosidase activity slows down the digestion of carbohydrates, thereby reducing glucose absorption into the blood and controlling blood sugar levels. Acarbose has been known as an inhibitor to have good activity in inhibiting α-glucosidase.[10,11] It binds very well to the α-glucosidase active site compared to the native substrate (α-glucose, disaccharides, and oligosaccharides). As a result, the carbohydrate hydrolysis pathway at the α-glucosidase active site can be stopped.[11] Therefore, the development of α-glucosidase inhibitors needs to be studied to find more efficient drug candidates. Previous studies showed that coumarin derivatives played a promising role in inhibiting the activity of α-glucosidase.[12–14] One of them is nordentatin, where nordentatin is the majority secondary metabolite compound of *Clausena excavata*. This compound was modified using a semi-synthetic method into ester derivatives to develop anti-diabetic candidates.[14] The availability of nordentatin from natural products has advantages in anti-diabetic development. Therefore, the study of structural modification becomes crucial in developing anti-diabetic candidates. As reported by our previous work, structural modification of nordentatin through the semi-synthetic reaction of pyranocoumarin can increase the inhibitory activity of the α-glucosidase compared to acarbose (IC_{50}: 7.57 mM) as the positive control. Some of them, namely PC1 (IC_{50}: 1.54 mM), PC2 (IC_{50}: 4.87 mM), and PC3 (IC_{50}: 2.43 mM).[14] Based on the report, three semi-synthetic pyranocoumarin derivatives (Fig. 1) are selected as the main focus in this study for further study of the mechanism of α-glucosidase inhibition at the molecular level.

The structure-based approach is known as one of the reliable *in silico* approaches. It helps predict free energy binding (ΔG_{bind}) between ligands and targeted proteins. The advantage alternative that can be offered is to combine molecular docking and molecular dynamics (MD) simulation, which can predict the value of ΔG_{bind} more accurately in representing the ligand-receptor binding affinity. The ΔG_{bind} can be calculated using two approaches, namely conventional (MM) and hybrid (QM/MM). Conventional or molecular mechanics are computational approaches that are often relied upon in ΔG_{bind} calculation. This approach can be used through two solvent models, such as Poisson-Boltzmann surface area (PBSA) and generalized Born surface area (GBSA).[15] It is known that the PBSA solvent model takes considerable computation time compared to GBSA. Therefore, the GBSA solvent model attracts more attention for further development in ΔG_{bind} calculations for several computing systems. One way is to use a hybrid approach with the GBSA solvent model. In the QM approach, the internal energy is calculated using several basis sets, such as PM3 and DFTB methods. However, the DFTB method requires a high computational cost compared to the PM3 method. Additionally, the QM method is focused on the ligand, whereas the MM method is focused on the receptor. The application of this approach in conducting ΔG_{bind} analysis has proven to be successfully applied to many systems.[16] Therefore, the prediction of ΔG_{bind} values can be calculated through the Quantum Mechanic/Molecular Mechanic-Generalized Born Surface Area (QM/MM-GBSA) approach. Its calculated prediction can detail the ΔG_{bind} values of each system, such as ligand, receptor, and complex.[15] Additionally, the calculation of ΔG_{bind} using a hybrid approach (QM/MM) is considered to have better prediction accuracy than the conventional approach (MM). The expectancy is that the prediction of ΔG_{bind} using this method has a level of accuracy close to the experimental results.

Structural units and functional groups affect the activity of a drug candidate through a series of targeted protein-inhibitory mechanisms in the human body. Therefore, molecular studies play a crucial role in understanding the inhibitory mechanism of a drug candidate.[17] The goal is to be able to determine the key binding residue that plays regulation in the inhibition of the target protein. In addition, the advantages of molecular studies are being able to provide promising lead compounds to be continued in modifying functional groups through semi-synthesis methods. In this present study, we tried to study the inhibitory mechanism of pyranocoumarin derivatives (PC1, PC2, and PC3), which have good inhibitory activity against the α-glucosidase at the molecular level through computational

studies. Molecular studies regarding the activity of pyranocoumarin derivatives (PC1, PC2, and PC3) against α-glucosidase are first reported in this paper. Several main variables measured in this study are conformational dynamics, binding affinity, and key binding residue. The information and data obtained from this study are expected to be a reference for future drug designs based on pyranocumarin compounds.

Methodology

Ligand and receptor preparation

The inhibition target selected in this study was the α-glucosidase enzyme from *Saccharomyces cerevisiae*. Meanwhile, the selection of the protein code: 3A4A for the α-glucosidase enzyme is obtained from the protein data bank (**https://www.rcsb.org/structure/3a4a**). The selected protein is a crystal complex of the α-glucosidase enzyme successfully characterized from *Saccharomyces cerevisiae*.[4] Reconstruction of the standard missing residue using the modeller 9.21 package. In addition, at the α-glucosidase active site, there is a native ligand, namely α-D-glucopyranose (PDB ID: GLC). The GLC coordinates were used as a reference for determining the α-glucosidase active site. Acarbose is also performed in this study as a control. Meanwhile, the pyranocoumarin derivatives (PC1, PC2, and PC3) modeled in this study have been successfully synthesized and characterized by previous studies.[14] For the preparation of pyranocoumarins, the electrostatic potential (ESP) charges were calculated using semiempirical quantum parametric method-3 (SQM-PM3) *via* Gaussian 16 package.[18] Additionally, the addition of hydrogen atoms, AMBER FF14SB force field, and AM1-BCC aims to calculate missing parameters, such as bonded, non-bonded, and charge.

Molecular docking

All stages of molecular docking were performed using the DOCK6 package.[19] The cluster sphere is determined using the *sphgen* tool to find the coordinates of the receptor active site. Furthermore, native ligand coordinates are used to select cluster spheres with a radius of 10.0 Å based on GLC ligand coordinates using the sphere_selector tool. The selected cluster sphere is used as a coordinate where ligand and receptor interaction occurs. Grid-box preparation uses several crucial parameters, such as grid-spacing (0.3 Å), center (X: 20.53, Y: −10.11, Z: 22.38), and dimensions (X: 27.31, Y: 29.51, Z: 29.35). Meanwhile, the interaction energy of ligand-α-Glu was calculated using a functional gird scoring with an anchor-and-grow algorithm.[20] The ligand-receptor scoring process (Eqn. (1)) takes place in the gaseous state with energy considerations in the form of van der Waals (E_{vdW}) and electrostatic (E_{ele}) energies.

$$\text{Grid-Score} = E_{vdW} + E_{ele} \quad (1)$$

System preparation for MD simulation

The topology preparation before the simulation is carried out through the tleap tool[21] contained in the AMBER22 package, which consists of ligand, receptor, solvated receptor, complex, and solvated complex topologies. The ligand topology is prepared using the parmchk tool to generate a frcmod file containing bond, angle, dihedral, improper, and non-bond parameters. The preparation of receptor topology consists of standard amino acids with the leaprc_source_protein tool based on force field ffSB14.[22] The complex topology combines the ligand and receptor coordinates obtained previously using the amberparm tool available in the AMBER22 package. Meanwhile, the solvated topologies are applied through solvatebox TIP3PBOX (distance: 12 Å) with the leaprc.water.tip3p tool. The addition of sodium ions (Na^+) is done to neutralize the system randomly. Then, the system minimization is performed in three stages, that are (i) water molecules and sodium ions, (ii) ligand-receptor, and (iii) the whole system. The crucial parameters in the minimization process are the steepest descent: 1500 steps and conjugate gradient: 500 steps. Finally, the minimization process is calculated using the sander tools available in the AMBER22 package. The minimization process aims to keep the formed system does not experience excessive fluctuations during the simulation process due to the influence of bad atomic contacts.[23]

MD simulation

The simulation process is carried out through several stages, followed by heating, equilibrium, and production using PMEMD.cuda tool contained in the AMBER22 package. First, the heating stage is carried out for 200 ps with temperature settings from 10 K to 310 K gradually. Second, the system is equilibrated for 1300 ps at a temperature of 310 K in stages with harmonic restraints of 30, 20, 10, and 5 $kcal^{-1}\ mol^{-1}\ A^2$. Third, the production stage is carried out for 100 ns under NPT ensemble conditions (1 atm and 310 K). Furthermore, the trajectories generated during the simulation process are analyzed using cpptraj[24] and MMPBSA.py[15] tools, which are available in the AMBER22 package. Trajectories analysis is used to analyze several variables, such as conformational dynamics, binding affinity, key binding residue, inhibitor-α-glucosidase interaction, and water accessibility.

Free energy binding

The calculation of free energy binding $\Delta(G_{bind})$ uses the last 20 ns (80–100 ns) of trajectories with a hybrid-based approach. The enthalpy (ΔH) term is calculated by using the Quantum Mechanics/Molecular Mechanics-Generalized Born (QM/MM-GBSA) approach.[25] Furthermore, several crucial parameters, such as the generalized Born solvation model: 5 and QM level theory: PM3 method, were utilized in this work. Meanwhile, the entropy change ($-T\Delta S$) term is calculated based on the normal mode approach (NMODE). In summary, the ΔG_{bind} can be calculated through eqn (2). Free energy decomposition ($\Delta G_{bind}^{residue}$) is also calculated to find the interaction energy

between the ligand and the amino acid residue responsible for the interaction on the receptor active site. The $\Delta G_{\text{bind}}^{\text{residue}}$ calculation is calculated using the Molecular Mechanics-Generalized Born (MM-GBSA) approach. Meanwhile, the experimental ΔG_{bind} calculation uses eqn (3), the IC_{50} value as a reference variable.[26] The variables R and T are the ideal gas constant (1.9872×10^{-3} kcal K^{-1} mol^{-1}) and room temperature (300 K), respectively.

$$\Delta G_{\text{bind}} = \Delta H - T\Delta S \quad (2)$$

$$\Delta G_{\text{exp}} = R.T.\ln(IC_{50}) \quad (3)$$

Results and discussion

Molecular docking analysis

The molecular docking aims to determine the initial orientation of each ligand on the targeted protein active site. The molecular docking stage begins with determining the active site through the redocking method. This step has advantages in determining the active site of targeted proteins very well.[27] It should be noted that the coordinates of the native ligand obtained from the co-crystal are known. Briefly, GLC coordinates have been extracted using the chimera version 13 package. The cluster spheres on the receptor surface are shown in Fig. S1.† It shows that each color of the cluster spheres indicates the possible coordinates of the interactions on the receptor surface. The selection of spheres clusters is based on the GLC coordinates as the native ligand of the α-glucosidase. The redocking shows a good superposition with an RMSD value of 0.99 Å (Fig. 2). It also identified that the superposition of the redocking result (pose) gave coordinate values similar to the native ligand from the co-crystal.[19,20,28] Hence, the obtained coordinate from redocking is feasible for further analysis.

The second stage is to dock the ligand to the α-glucosidase active site. The variables measured at this stage are energy and type of interaction on the receptor active site. Docking results show that each ligand is well occupied to the receptor active site. Several amino acid residues are responsible for the interaction process for each ligand, such as GLC-α-Glu: eight, AC1-α-Glu: seven, PC1-α-Glu: six, PC2-α-Glu: seven, and PC3-α-Glu: seven (Fig. S2†). In particular, the pyranocoumarin derivatives, which are this study's main focus, show several interactions with amino acid residues on the receptor active site. In detail, PC1-α-Glu (K153, Y155, F300, F311, R312, and N412), PC2-α-Glu (K153, Y155, H277, F300, F311, R312, and D349), and PC3-α- Glu (K153, Y155, H277, F300, F311, R312, and N412). More specifically, the hydrogen bond shows that PC1-α-Glu and PC3-α-Glu have one hydrogen bond with the residue N412. Meanwhile, PC2-α-Glu did not show any hydrogen bonds. This finding will be discussed further in the next section to look at the hydrogen bond occupation of pyranocoumarin derivatives. The interaction energy showed that the pyranocumarins have a better grid score than acarbose and GLC (Fig. 3). This result is indicated by the increasingly negative value of the grid score (kcal mol^{-1}). The grid score value is obtained from the contribution of energy in the gas phase, namely van der Waals (E_{vdW}) and electrostatic (E_{ele}) energies. In particular, E_{vdW} shows a significant energy contribution (>−60.00 kcal mol^{-1}) to the interaction energy of pyranocoumarins against α-glucosidase. Overall, the grid score analysis showed an inhibitory activity (IC_{50}) which is similar to the results of the *in vitro* test that we previously reported,[14] PC1 > PC3 > PC2 > AC1. We assume that the contribution of E_{vdW} has a significant contributor to the interaction energy between pyranocumarins and α-glucosidase, thermodynamically. It should be noted that this assumption needs to be studied further through the MD simulation, which is explained in detail in the next section. Therefore, the analysis of pyranocoumarins (PC1, PC2, and PC3) is feasible to study their dynamic behavior. This consideration was taken based on its excellent inhibitory activity against the α-glucosidase in the form of IC_{50} and grid score values. The obtained coordinates from molecular docking were used for further analysis, such as conformational dynamics, binding affinity, key binding residue, water accessibility, and inhibitor-α-glucosidase interaction.

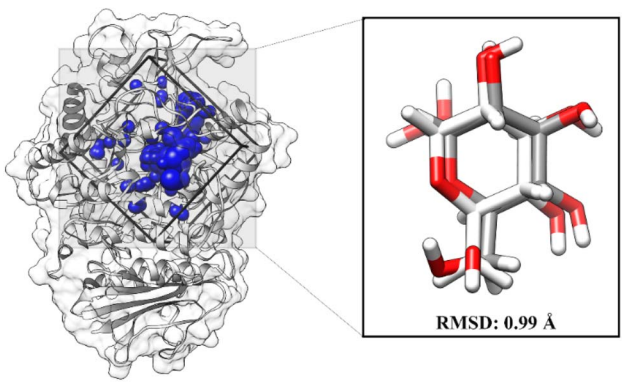

Fig. 2 Redocking analysis: the grid-box coordinate is based on the selected cluster sphere. The GLC superposition between co-cristal (white) and pose (grey).

Conformational dynamics of each system: stability, compactness, and flexibility

For the conformational dynamics evaluation of each system, we use 100 ns trajectories to analyze several variables, such as the root-mean-square displacement (RMSD), total energy, the radius of gyration (RoG), B-factor, and the root-mean-square fluctuations (RMSF). These variables aim to see the quality of each system.

The RMSD value identifies the system's stability formed during the simulation time.[29] Notably, the RMSD of each system showed insignificant fluctuation, which is <0.4 nm (Fig. 4). The RMSD value of each system rapidly increased during the first 2 ns and then fluctuated at ~0.19–0.25 nm in all systems until 100 ns. In particular, the last 40 ns trajectories (60–100 ns) show good stability. From the thermodynamic aspect, the total energy also shows that each system has converged because it does not have excessive energy fluctuations during the heating, equilibrium, and production stages under NPT assembly. It can be

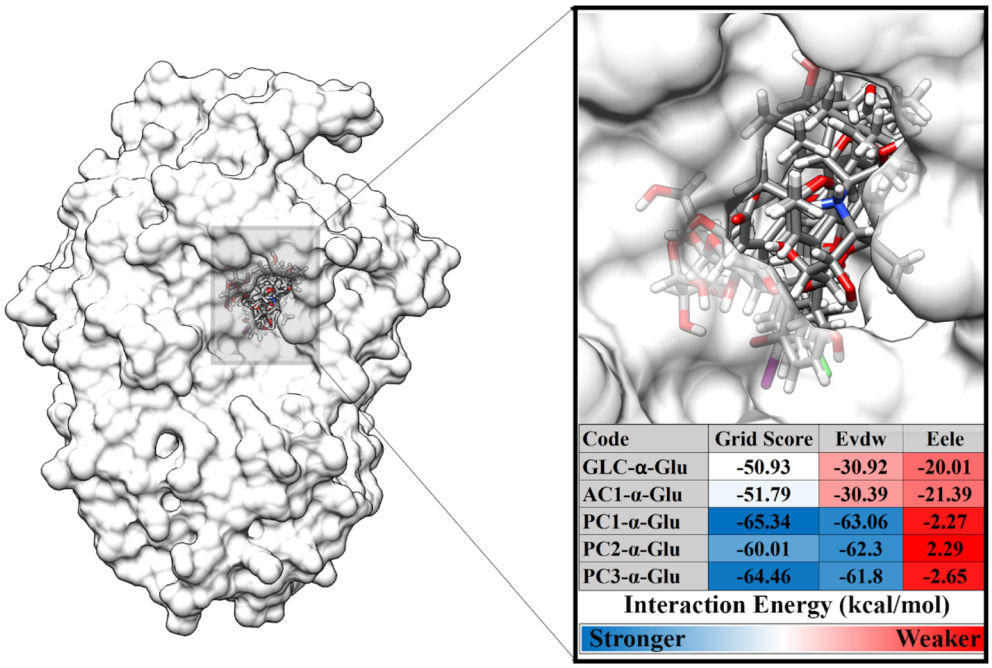

Fig. 3 Ligand-receptor docking based on grid score functional (E_{vdW} + E_{ele}).

seen through the fluctuation plot (Fig. S3†) and the average value (Table S1†) of the total energy.

The analysis continued to see the compactness of the formed structure during the simulation through RoG analysis. In tune with system stability, the RoG value showed insignificant fluctuation for each system (Fig. 4). Overall, the RoG values showed an average fluctuation at ~2.41–2.42 nm. The insignificant difference in RoG values indicates that each system's structure is rigid and stably folded.[30] This statement is supported by looking at the average structure during 100 ns simulation time (Fig. 5). On the opposite, we also analyze the flexibility of each system (Fig. 5) through B-factor and RMSF values.[31] The analysis shows that the apoprotein structure is more flexible than the three formed complexes. We suggest that pyranocumarins that bind to the receptor active site can increase the rigidity of the complex. It can be seen from the average values of the B-factor and RMSF, which show a flexibility trend as follows α-Glu > PC1-α-Glu > PC2- α-Glu > PC3- α-Glu (Table S1†).

The conformational dynamics analysis shows that each system has reached its equilibrium and is suitable for further analysis. Based on the stability analysis that has been described, we use the last 10 ns trajectories to calculate free energy binding and energy decomposition.

Binding affinity of inhibitors against α-glucosidase

Free energy binding (ΔG_{bind}) was calculated using the *MMPBSA.py* tool available in the AMBER22 package. The ΔG_{bind} calculation uses 100 snapshots extracted from the last 10 ns trajectories. It is because system stability has been achieved on its trajectories range (Fig. 4). In addition, the pyranocoumarins superposition extracted from the trajectories range does not experience a significant change in coordinates on the receptor

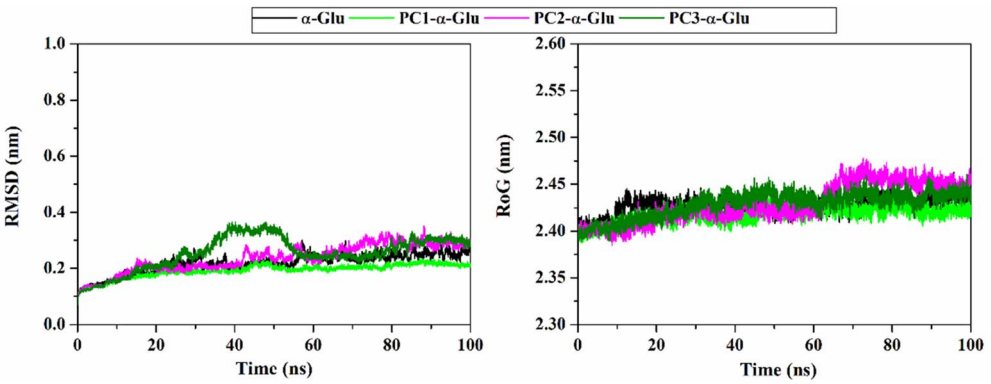

Fig. 4 The root-mean-square displacement of all atoms (left) and radius of gyration (right) for each system plotted along the 100 ns simulation time.

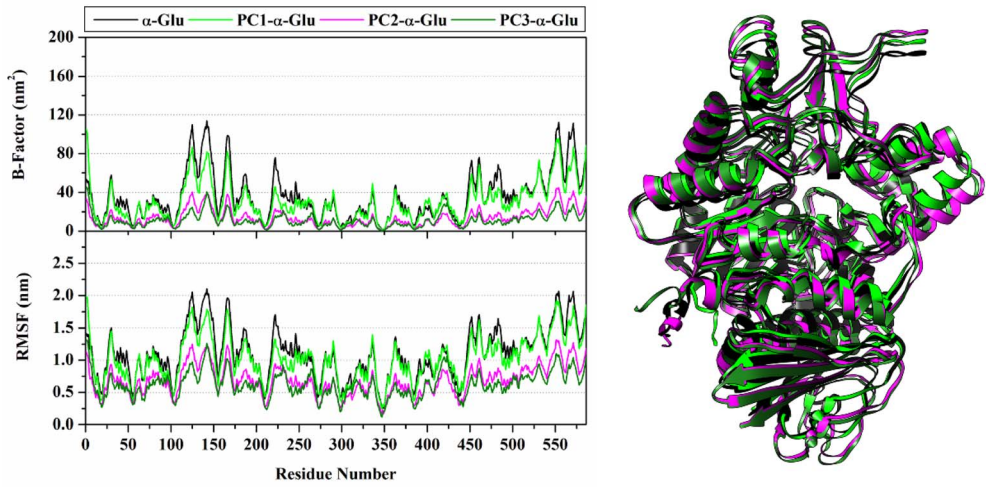

Fig. 5 System flexibility is shown by B-factor and the root-mean-square fluctuations (left) and the superposition of average structure (right) plotted along 100 ns simulation time.

active site (Fig. 6). Therefore, visualization data is the indicator that considered to analyze the ΔG_{bind} of each system. In detail, Energy component calculations from ΔG_{bind} are listed in Table 1.

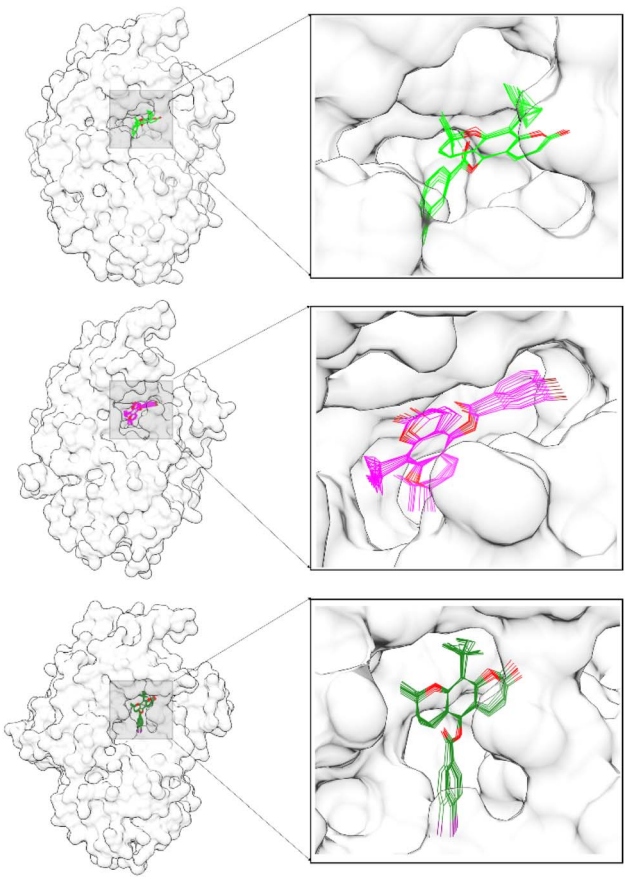

Fig. 6 The ligand superposition on the α-glucosidase active site was extracted in 10 snapshots from the last 10 ns trajectories: PC1-α-Glu (top), PC2-α-Glu (middle), and PC3-α-Glu (bottom).

The enthalpy energy component (ΔH) is divided into two main categories, that is, gas (ΔG_{gas}) and solvation (ΔG_{sol}) terms.[32] In detail, the ΔG_{gas} term is obtained from the contribution of van der Waals (ΔE_{vdW}) and electrostatic (ΔE_{ele}) energies.[33,34] Meanwhile, the ΔG_{sol} term is obtained from the contribution of the generalized Born model (ΔG_{solv}^{ele}) and solvent-accessible surface area energy ($\Delta G_{solv}^{nonpolar}$). The results show that ΔG_{gas} is the most significant main contribution to ΔH for each system compared to ΔG_{sol}. More specifically, ΔE_{vdW} is the main contributor to the ΔG_{bind} value. It is inseparable from the results of molecular docking analysis, which show a similar trend. In particular, in calculations using the QM method, self-consistent energy (ΔG_{SCF}) also contribute to the ΔG_{bind} value of

Table 1 Energy components (kcal mol^{-1}) of each system were calculated by using QM/MM-GBSA approach. Data are shown as mean ± standard error of the mean (SEM)

Energy Components	PC1-α-Glu	PC2-α-Glu	PC3-α-Glu
QM/MM (PM3)			
ΔE_{vdW}	−50.53 ± 0.21	−42.96 ± 0.25	−50.48 ± 0.42
ΔE_{ele}	−0.30 ± 0.00	0.93 ± 0.00	0.68 ± 0.00
ΔG_{gas}	−50.83 ± 0.21	−42.03 ± 0.25	−49.79 ± 0.42
ΔG_{SCF}	−17.67 ± 0.29	−14.48 ± 0.63	−22.14 ± 0.61
GBSA			
ΔG_{solv}^{ele}	40.79 ± 0.32	33.50 ± 0.49	41.00 ± 0.51
$\Delta G_{solv}^{nonpolar}$	−6.43 ± 0.01	−5.16 ± 0.03	−6.07 ± 0.03
ΔG_{sol}	34.36 ± 0.31	28.34 ± 0.51	34.93 ± 0.50
NMODE			
$-T\Delta S$	20.17 ± 1.26	24.48 ± 0.98	23.32 ± 1.34
Hybrid-based free energy binding			
ΔH	−34.14 ± 0.27	−28.17 ± 0.26	−37.00 ± 0.46
ΔG_{bind}	−13.97	−3.69	−13.68
Experimental free energy binding			
ΔG_{exp}	−3.86	−3.17	−3.58

each system[33,35] It should be noted that the pyranocoumarin molecules are treated as a QM region using the SQM-PM3 method. Interestingly, the value of ΔG_{SCF} shows a significant difference for each system. It indicates that the differences in functional groups (Cl, Br, and I) in each pyranocoumarins significantly influence the ΔG_{SCF} value. Meanwhile, changes in entropy ($-T\Delta S$) make a crucial contribution to the value of free energy binding.[26] It can be seen through eqn (2), described in the previous section. Briefly, the free energy binding value (kcal mol^{-1}) shows a good correlation between the predicted (ΔG_{bind}) and experimental (ΔG_{exp}) results with the binding affinity strength as follows: PC1 > PC3 > PC2. Interestingly, the grid score from molecular docking also shows a similar trend (Fig. 3). Based on ΔG_{bind}, PC3 has –I (larger size) as a functional group showing better binding affinity in comparison to –Br (PC2). However, the PC1 having –Cl (smallest in size) is showing the best results. It should be noted that PC1, PC2, and PC3 structures have different halogen atoms on the 4″ and 5″ positions of the phenyl ring. Additionally, the difference in the size of the halogen atom can increase the possibility of interaction with amino acid residues on the α-glucosidase active site. Meanwhile, the difference in position leads to a change in the binding orientation of the phenyl ring in each inhibitor. Differences in size and position also affect the interaction energy of ΔG_{SCF}, ΔH, and $-T\Delta S$ (Table 1). These factors are the main reasons for determining the binding affinity of each system thermodynamically. Systems with a more substantial ΔG_{bind} value are expected to bind well on the α-glucosidase active site and inhibit the regulation of carbohydrate hydrolysis into glucose monomers by this enzyme.

Key binding residues

In this section, we suspect several key binding residues are the main contributors to stabilizing the pyranocoumarins binding. Therefore we evaluated the decomposition energy ($\Delta G_{bind}^{residue}$) using the MM-GBSA approach.[15] The calculation of $\Delta G_{bind}^{residue}$ aims to study the interaction energy of amino acids that are at the receptor active site.[33] Meanwhile, consideration of interaction energy criteria is indicated by the value of $\Delta G^{residue}_{bind} < -1.00$ kcal mol^{-1}. The value of $\Delta G_{bind}^{residue}$ is obtained from the energy contribution of E_{vdw} and E_{ele} for each residue. The results show that each system has key bindingresidues that meet the criteria (Fig. 7), such as PC1-α-Glu (three residues:

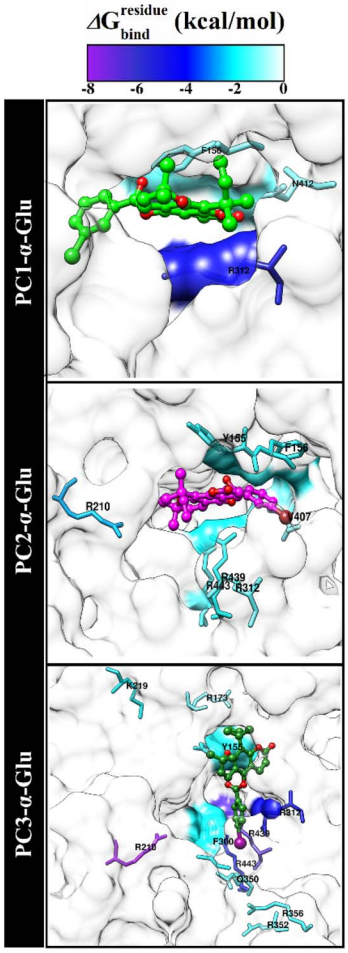

Energy contribution (kcal/mol)

Stronger ... Weaker

Residues	E_{Total}	E_{vdW}	E_{ele}
PC1-α-Glu			
F156	-1.31	-1.72	0.41
R312	-5.11	-3.88	-1.23
N412	-1.19	-0.34	-0.85
PC2-α-Glu			
Y155	-1.79	-4.36	2.56
F156	-1.94	-2.23	0.29
R210	-2.63	-0.04	-2.59
R312	-1.35	-0.31	-1.04
V407	-1.02	-0.80	-0.22
R439	-1.87	-0.14	-1.73
R443	-1.64	-0.02	-1.62
PC3-α-Glu			
Y155	-1.70	-4.39	2.69
R173	-1.31	-0.02	-1.28
R210	-8.98	-0.02	-8.97
K219	-2.04	-0.01	-2.03
F300	-1.87	-2.50	0.64
R312	-4.80	-2.82	-1.98
Q350	-1.32	-0.58	-0.74
R352	-1.47	-0.01	-1.47
R356	-1.51	-0.07	-1.44
R439	-6.54	-0.10	-6.44
R443	-3.89	-0.01	-3.88

Fig. 7 The energy decomposition ($\Delta G_{bind}^{residue}$) and energy contribution ($E_{vdW} + E_{ele}$) were calculated by using the MM-GBSA approach. The results were plotted over the last 10 ns trajectories.

F165, R312, and N412), PC2-α-Glu (seven residues: Y155, F156, R210, R312, V407, R439, and R443), and PC3-α-Glu (eleven residues: Y155, R173, R210, R219, F300, R312, Q350, R352, R356, R439, and R443). In particular, PC1-α-Glu shows that the residue R312 has $\Delta G_{\text{bind}}^{\text{residue}}$, which is −5.11 kcal mol^{-1}. It identifies that the residue is favorable to PC1 bindings. In addition, we suspect that residue N412 is leading for PC1 bindings because it has several crucial interactions, such as atomic contact and hydrogen bond, which will be explained in the next section. In the case of PC3-α-Glu, showing amino acid residues that have a substansial $\Delta G_{bind}^{\text{residue}}$ contribution, that is, R210 (−8.98 kcal mol^{-1}), R312 (−4.80 kcal mol^{-1}), and R439 (−6.54 kcal mol^{-1}). The presence of the –I atom on the 5″ position of phenyl contributes to stabilizing three key binding residues, namely F300, R312, and Q350 (Fig. 7). It is seen that the phenyl-5″-I ring enters and binds the receptor pocket very well (Fig. 6). The –I atom size may influence the binding orientation of the PC3 molecule.

Therefore, the presence of the –I atom on the 5″ position of phenyl is crucial in stabilizing the interaction in the receptor active site. Meanwhile, PC2-α-Glu showed a contribution of $\Delta G_{\text{bind}}^{\text{residue}}$ from −1.02 to −2.63 kcal mol^{-1}. It is hoped that the information obtained from the key binding residue can lead us to understand the binding pattern of the ligand-receptor.[23] It is helpful as a reference for consideration in the rational selection of functional groups in obtaining reliable candidate α-glucosidase inhibitors.

Inhibitor-α-glucosidase interaction in the binding pocket

For the following evaluation, we tried to describe the interaction between the pyranocoumarins and the α-glucosidase at the atomistic level. Here we describe two main variables, namely atomic contact and hydrogen bond. Those variables are analyzed using 100 ns trajectories. The results show that each system has intense contact atoms with several amino acid residues on the receptor active site (Fig. 8 and Table S2†), namely PC1-α-Glu: 13 contacts, PC2-α-Glu: 18 contacts, and PC3-α-Glu: 10 contacts. Furthermore, we found that among the amino acid residues, several key binding residues have intense contact with each of the pyranocoumarins. In particular, residue N412, one of the key binding residues, experienced intense contact with oxygen atoms (2C=O) from PC1 by 92.39% during a simulation time of 100 ns. Furthermore, we analyzed the hydrogen occupation for each system (Table 2). Hydrogen bonds with an acceptable percentage of $P_{\text{HB}} \geq 90\%$ identify the strong category.[36] Once again, occupation N412 shows a good hydrogen bond category with P_{HB} equal to 90.88%. This finding reinforces our previous assumptions about residue N412 as a guide for the binding pattern of PC1-α-Glu. In another site, PC3-α-Glu showed a P_{HB} value of 19.25% for residue N412 with a weak hydrogen bond category. Meanwhile, PC2-α-Glu did not show hydrogen bond criteria even though two bonds were recorded with residue R312 during a simulation time of 100 ns. It is because the two bonds have a tiny percentage of hydrogen bond occupation, which is <10%. This finding shows a correlation with the results of molecular docking (Fig. S2†). It might explain why PC2 has lower inhibitory activity than the other two pyranocoumarin derivatives. Therefore, the selection of functional groups greatly influences the binding orientation of a molecule.

Table 2 The hydrogen bond was calculated using 100 ns trajectories (the cut value: distance 3.5 Å and angle 120°)

H-Bond	P_{HB} (%)	AvgDist (Å)	AvgAng (°)
PC1-α-Glu			
2C=O···H–ND2(N412)	90.88	3.04	153.10
PC2-α-Glu			
1″C=O···H–NH1(R312)	1.43	3.25	126.54
8C–O···H–N(R312)	1.10	3.37	160.63
PC2-α-Glu			
2C=O···H-ND2(N412)	19.25	3.08	151.98

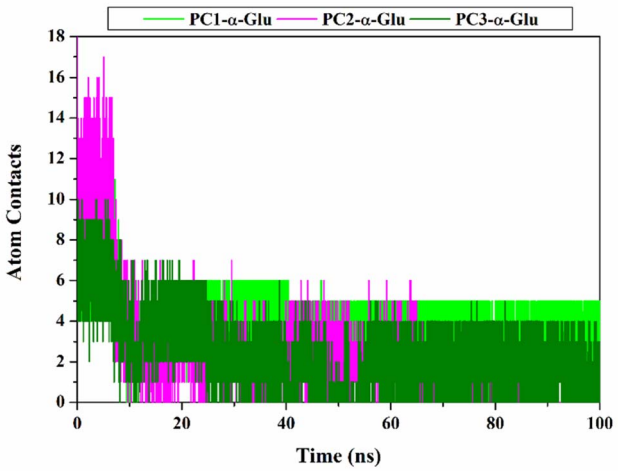

Fig. 8 Inhibitor- α-glucosidase interaction: Atom contacts was plotted along 100 ns simulation time.

Water accessibility of inhibitor-α-glucosidase

The water molecules to access the receptor surface area were presented through the solvent-accessible surface area (SASA).[37,38] The analysis process uses 100 ns trajectories during the simulation time (Fig. 9). In particular, the solvent access to the receptor pocket uses a radius of 5 Å from the coordinates of each ligand. The obtained results show the access value of water molecules for each system, followed by PC2-α-Glu > PC3-α-Glu > PC1-α-Glu (Table 3). We suspect that the difference in SASA values in each system is caused by differences in the size (–Cl, –Br, and –I) and position (meta/para) of the functional groups of each molecule. The difference in SASA values in the pocket surface area indicates that the difference in size and position of the halogen atoms can impact the water molecule's access. In general, access to water molecules can be affected by a ligand in the receptor pocket area.[39] It is caused by the lack of free space in the pocket surface area to be accessed by water molecules. Meanwhile, the functional group position can change the

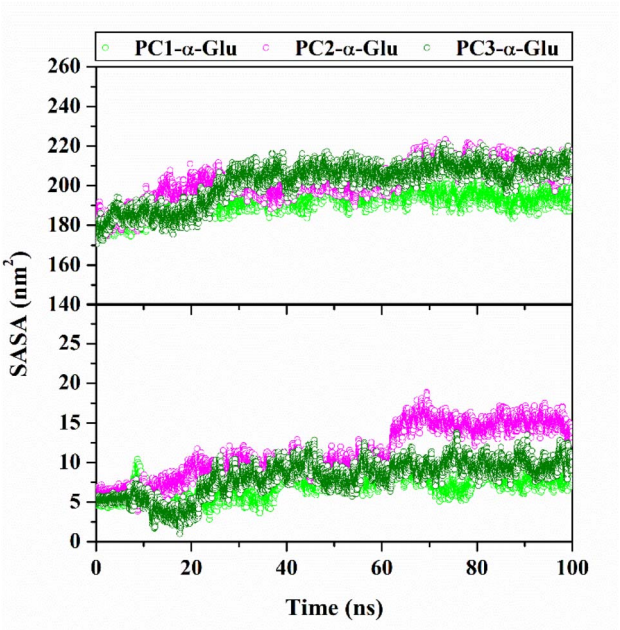

Fig. 9 The solvent-accessible surface (SASA) plotted along 100 100 ns simulation time: All surface area (top) and pocket surface area (bottom).

Table 3 The average value of SASA was calculated using 100 ns trajectories

System	All surface area (nm^2)	Pocket surface area (nm^2)
PC1-α-Glu	192.65 ± 5.65	7.07 ± 1.43
PC2-α-Glu	202.28 ± 8.86	11.14 ± 3.32
PC3-α-Glu	201.77 ± 10.33	8.09 ± 2.19

orientation of a molecule in the binding pattern. Consequently, this orientation affects the number of water molecules to access the pocket surface area. As we know, the role of water molecules is crucial for maintaining protein structure.[40]

Conclusions

In this work, we describe the differences in the inhibitory activity of three pyranocoumarin derivatives (PC1, PC2, and PC3) against the α-glucosidase enzyme at the molecular level. The analysis process is carried out through a structure-based approach in the form of molecular docking and molecular dynamics simulation. We found that the differences in the functional groups and the positions of the halogen atoms in the modeled molecular structures lead to differences in the inhibitory activity of the α-glucosidase. The simulation results suggest that pyranocoumarins that bind to the receptor active site can increase the rigidity and stability of the complex. From the thermodynamic aspect, the binding affinity calculation shows a good correlation with the predicted and experimental free energy binding value, following the trend of PC1 > PC3 > PC2. Meanwhile, we found that there are 15 key binding residues ($\Delta G_{bind}^{residue}$) that play a role in stabilizing the pyranocoumarins binding, such as Y155, Y156, F165, R173, R210, R219, F300, R312, Q350, R352, R356, V407, N412, R439, and R443. Hopefully, obtained information from this work can provide insight into designing candidates for α-glucosidase enzyme inhibitors based on pyranocoumarin derivatives.

Author contributions

M. I. A conceived the *in silico* research, analyzed the results, wrote the initial manuscript, and finalized the manuscript. I. S. and B. S. contained computational resources. N. S. A and A. N. K. supervised the research and revised the manuscript. A. P. W and Y. T. helped with the supervised data collection. All authors discussed and commented on the manuscript.

Conflicts of interest

The authors declare no conflict of interest.

Acknowledgements

This study was supported by the Research Program of "Penelitian Pasca Sarjana – Penelitian Disertasi Doktor" from DRTPM KEMENDIKBUDRISTEK TAHUN 2022. Contract Number: 923/UN3.15/PT/2022. Additionally, we are grateful for this work's computational resources supported by UCoE Research Center for Bio-Molecule Engineering, Universitas Airlangga (BIOME-UNAIR).

References

1 T. Tian, G. Y. Chen, H. Zhang and F. Q. Yang, *Molecules*, 2021, **26**, 1–11.
2 D. R. Rose, M. M. Chaudet and K. Jones, *J. Pediatr. Gastroenterol. Nutr.*, 2018, **66**, S11–S13.
3 F. J. Pasquel, M. C. Lansang, K. Dhatariya and G. E. Umpierrez, *Lancet Diabetes Endocrinol.*, 2021, **9**, 174–188.
4 K. Yamamoto, H. Miyake, M. Kusunoki and S. Osaki, *FEBS J.*, 2010, **277**, 4205–4214.
5 U. Ghani, *Eur. J. Med. Chem.*, 2015, **103**, 133–162.
6 C. Proença, M. Freitas, D. Ribeiro, E. F. T. Oliveira, J. L. C. Sousa, S. M. Tomé, M. J. Ramos, A. M. S. Silva, P. A. Fernandes and E. Fernandes, *J. Enzyme Inhib. Med. Chem.*, 2017, **32**, 1216–1228.
7 A. M. Dirir, M. Daou, A. F. Yousef and L. F. Yousef, *Phytochem. Rev.*, 2022, **21**, 1049–1079.
8 U. Hossain, A. K. Das, S. Ghosh and P. C. Sil, *Food Chem. Toxicol.*, 2020, **145**, 111738.
9 S. T. Assefa, E. Y. Yang, S. Y. Chae, M. Song, J. Lee, M. C. Cho and S. Jang, *Plants*, 2020, **9**, 1–17.
10 J. J. DiNicolantonio, J. Bhutani and J. H. O'Keefe, *Open Heart*, 2015, **2**, e000327.
11 L. Gong, D. Feng, T. Wang, Y. Ren, Y. Liu and J. Wang, *Food Sci. Nutr.*, 2020, **8**, 6320–6337.

12 T. M. Thant, N. S. Aminah, A. N. Kristanti, R. Ramadhan, P. Phuwapraisirisan and Y. Takaya, *Nat. Prod. Res.*, 2021, **35**, 556–561.
13 A. Athipornchai, R. Kumpang and S. Semsri, *J. Oleo Sci.*, 2021, **70**, 1669–1676.
14 T. M. Thant, N. S. Aminah, A. N. Kristanti, R. Ramadhan, H. T. Aung and Y. Takaya, *Open Chem.*, 2020, **18**, 890–897.
15 B. R. Miller, T. D. McGee, J. M. Swails, N. Homeyer, H. Gohlke and A. E. Roitberg, *J. Chem. Theory Comput.*, 2012, **8**, 3314–3321.
16 T. Hou, J. Wang, Y. Li and W. Wang, *J. Chem. Inf. Model.*, 2011, **51**, 69–82.
17 Q. Li and C. Kang, *Int. J. Mol. Sci.*, 2020, **21**, 1–18.
18 M. J. Frisch, G. W. Trucks, H. B. Schlegel, G. E. Scuseria, M. A. Robb, J. R. Cheeseman, G. Scalmani, V. Barone, B. Mennucci, G. A. Petersson, H. Nakatsuji, M. Caricato, X. Li, H. P. Hratchian, A. F. Izmaylov, J. Bloino, G. Zheng, J. L. Sonnenberg, M. Hada, M. Ehara, K. Toyota, R. Fukuda, J. Hasegawa, M. Ishida, T. Nakajima, Y. Honda, O. Kitao, H. Nakai, T. Vreven, J. A. Montgomery, Jr., J. E. Peralta, F. Ogliaro, M. Bearpark, J. J. Heyd, E. Brothers, K. N. Kudin, V. N. Staroverov, R. Kobayashi, J. Normand, K. Raghavachari, A. Rendell, J. C. Burant, S. S. Iyengar, J. Tomasi, M. Cossi, N. Rega, J. M. Millam, M. Klene, J. E. Knox, J. B. Cross, V. Bakken, C. Adamo, J. Jaramillo, R. Gomperts, R. E. Stratmann, O. Yazyev, A. J. Austin, R. Cammi, C. Pomelli, J. W. Ochterski, R. L. Martin, K. Morokuma, V. G. Zakrzewski, G. A. Voth, P. Salvador, J. J. Dannenberg, S. Dapprich, A. D. Daniels, O. Farkas, J. B. Foresman, J. V. Ortiz, J. Cioslowski, and D. J. Fox, *Gaussian 16, Revision C.01*, Gaussian, Inc., Wallingford CT, 2016.
19 W. J. Allen, T. E. Balius, S. Mukherjee, S. R. Brozell, D. T. Moustakas, P. T. Lang, D. A. Case, I. D. Kuntz and R. C. Rizzo, *J. Comput. Chem.*, 2015, **36**, 1132–1156.
20 S. R. Brozell, S. Mukherjee, T. E. Balius, D. R. Roe, D. A. Case and R. C. Rizzo, *J. Comput.-Aided Mol. Des.*, 2012, **26**, 749–773.
21 D. A. Case, T. E. Cheatham, T. Darden, H. Gohlke, R. Luo, K. M. Merz, A. Onufriev, C. Simmerling, B. Wang and R. J. Woods, *J. Comput. Chem.*, 2005, **26**, 1668–1688.
22 J. A. Maier, C. Martinez, K. Kasavajhala, L. Wickstrom, K. E. Hauser and C. Simmerling, *J. Chem. Theory Comput.*, 2015, **11**, 3696–3713.
23 B. Nutho, S. Pengthaisong, A. Tankrathok, V. S. Lee, J. R. K. Cairns, T. Rungrotmongkol and S. Hannongbua, *Biomolecules*, 2020, **10**, 1–19.
24 D. R. Roe and T. E. Cheatham, *J. Chem. Theory Comput.*, 2013, **9**, 3084–3095.
25 A. S. Christensen, T. Kubař, Q. Cui and M. Elstner, *Chem. Rev.*, 2016, **116**, 5301–5337.
26 P. C. Su, C. C. Tsai, S. Mehboob, K. E. Hevener and M. E. Johnson, *J. Comput. Chem.*, 2015, **36**, 1859–1873.
27 E. D. Boittier, Y. Y. Tang, M. E. Buckley, Z. P. Schuurs, D. J. Richard and N. S. Gandhi, *Int. J. Mol. Sci.*, 2020, **21**, 1–19.
28 P. C. H. Lam, R. Abagyan and M. Totrov, *J. Comput.-Aided Mol. Des.*, 2018, **32**, 187–198.
29 M. Askarzadeh, H. Azizian, M. Adib, M. Mohammadi-Khanaposhtani, S. Mojtabavi, M. A. Faramarzi, S. M. Sajjadi-Jazi, B. Larijani, H. Hamedifar and M. Mahdavi, *Sci. Rep.*, 2022, **12**, 1–16.
30 M. Y. Lobanov, N. S. Bogatyreva and O. V. Galzitskaya, *Mol. Biol.*, 2008, **42**, 623–628.
31 A. Bornot, C. Etchebest and A. G. De Brevern, *Proteins: Struct., Funct., Bioinf.*, 2011, **79**, 839–852.
32 C. Wang, D. Greene, L. Xiao, R. Qi and R. Luo, *Front. Mol. Biosci.*, 2018, **4**, 1–18.
33 E. Wang, H. Sun, J. Wang, Z. Wang, H. Liu, J. Z. H. Zhang and T. Hou, *Chem. Rev.*, 2019, **119**, 9478–9508.
34 S. Genheden and U. Ryde, *Expert Opin. Drug Discovery*, 2015, **10**, 449–461.
35 S. K. Mishra and J. Koča, *J. Phys. Chem. B*, 2018, **122**, 8113–8121.
36 J. Kästner, H. H. Loeffler, S. K. Roberts, M. L. Martin-fernandez and M. D. Winn, *J. Struct. Biol.*, 2009, **167**, 117–128.
37 S. Zhang, Y. Wang, L. Han, X. Fu, S. Wang, W. Li and W. Han, *Front. Chem.*, 2021, **9**, 1–13.
38 S. Ahmed, M. C. Ali, R. A. Ruma, S. Mahmud, G. K. Paul, M. A. Saleh, M. M. Alshahrani, A. J. Obaidullah, S. K. Biswas, M. M. Rahman, M. M. Rahman and M. R. Islam, *Molecules*, 2022, **27**, 1–19.
39 C. Barillari, J. Taylor, R. Viner and J. W. Essex, *J. Am. Chem. Soc.*, 2007, **129**, 2577–2587.
40 T. Vajda and A. Perczel, *J. Pept. Sci.*, 2014, **20**, 747–759.